Earthquakes and Structures, *Vol. 7, No. 6 (2014) 1141-1169*
DOI: http://dx.doi.org/10.12989/eas.2014.7.6.1141

Seismic base isolation of precast wall system using high damping rubber bearing

Patrick L.Y. Tiong[*1], Azlan Adnan[2a], Ahmad B.A. Rahman[2b] and Abdul K. Mirasa[3c]

[1]*Seismology and Earthquake Engineering Division, Doshin Rubber Products (M) Sdn. Bhd., Lot PT 34252, Jalan Sekolah, Rantau Panjang, 42100 Klang, Selangor, Malaysia*
[2]*Department of Structure and Materials, Faculty of Civil Engineering, Universiti Teknologi Malaysia, 81310 Skudai, Johor, Malaysia*
[3]*Department of Civil Engineering, Faculty of Engineering, Universiti Malaysia Sabah, 88400 Kota Kinabalu, Sabah, Malaysia*

(Received July 27, 2014, Revised October 2, 2014, Accepted 18 October, 2014)

Abstract. This study is aimed to investigate the seismic performance of low-rise precast wall system with base isolation. Three types of High Damping Rubber Bearing (HDRB) were designed to provide effective isolation period of 2.5 s for three different kinds of structure in terms of vertical loading. The real size HDRB was manufactured and tested to obtain the characteristic stiffness as well as damping ratio. In the vertical stiffness test, it was revealed that the HDRB was not an ideal selection to be used in isolating lightweight structure. Time history analysis using 33 real earthquake records classified with respective peak ground acceleration-to-velocity (a/v) ratio was performed for the remaining two types of HDRB with relatively higher vertical loading. HDRB was observed to show significant reduction in terms of base shear and floor acceleration demand in ground excitations having a/v ratio above 0.5g/ms^{-1}, very much lower than the current classification of 0.8g/ms^{-1}. In addition, this study also revealed that increasing the damping ratio of base isolation system did not guarantee better seismic performance particularly in isolation of lightweight structure or when the ground excitation was having lower a/v ratio.

Keywords: high damping rubber bearing; seismic base isolation; precast wall; damping ratio; passive earthquake mitigation

1. Introduction

The conventional seismic resistance design approach posed a challenge for designers to obtain a balance between minimizing both floor accelerations and interstory drifts simultaneously in the designed structures (Mayes and Naeim 2001). It is understood that excessive interstory drifts can be eliminated by constructing a stiffer building. However, a stiffer building, which is now becoming less flexible, will cause high floor accelerations. In the other way round, a flexible

∗Corresponding author, Ph.D., E-mail: patrick@rubberdamping.com
[a]Professor, E-mail: azlanadnan@utm.my
[b]Associate Professor, E-mail: baharfka@utm.my
[c]Professor, E-mail: irdrakm@gmail.com

http://www.techno-press.org/?journal=eas&subpage=7 ISSN: 2092-7614 (Print), 2092-7622 (Online)

Fig. 1 High damping rubber bearing (HDRB) showing internal layers

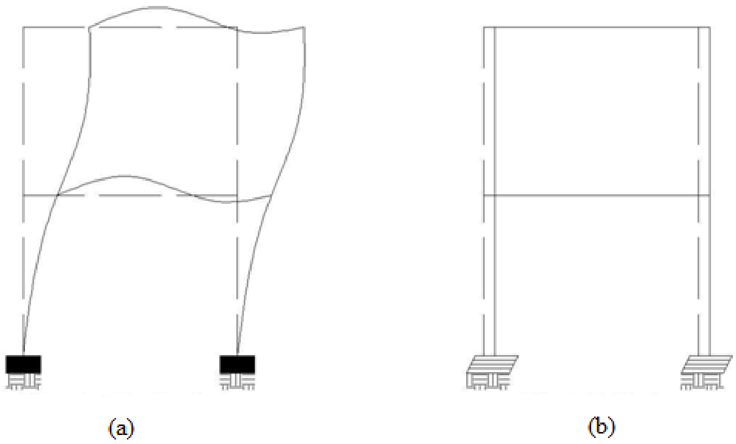

Fig. 2 Structural response of (a) fixed base and (b) base isolated structure

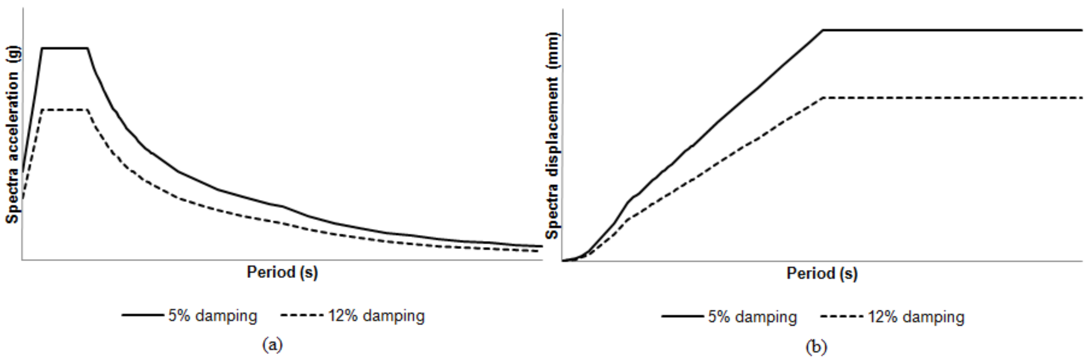

Fig. 3 Damping ratio effect on spectra (a) acceleration and (b) displacement

structure, though it will lead to lower floor accelerations, it causes large interstory drifts. Both the two factors cause greater force demand from either the building structural component or its contents within.

Earthquake itself normally does not cost lives but the collapsed structures do. The earthquake forces are generated within the structural system of a particular building due to the inertia of the structure when it reacts to the ground dynamic motion. In other words, the heavy mass of the building which reacts oppositely to counter the ground movement causes effective base shear as the restraining force transmitted from the ground to the top of structure. With such understanding of earthquake force transmission, separating the structure from ground could be an alternative to minimize such inertia response due to ground movement, termed as seismic base isolation. Thus, seismic base isolation has been proposed, studied and investigated by numerous researchers all over the world over the past decades as an alternative to the conventional ductility design concept. Although the earliest recorded history of seismic base isolation was as early as 1909, the growth of its application was not too apparent only until early 1980's with the development of multilayered elastomeric rubber bearing base isolators (Naeim and Kelly 1999).

There are varieties of devices available for seismic isolation of structures such as rollers, friction slip plates, capable suspension, sleeved piles and rocking foundations. Nevertheless, an elastomeric rubber bearing appears to be one of the most practical and widely used seismic base isolation systems (Forni 2010, Warn and Ryan 2012). Figure of an elastomeric rubber bearing, or sometimes termed as high damping rubber bearing (HDRB) or laminated rubber bearing is shown in Fig. 1.

The basic concept of seismic base isolation is to decouple the superstructure from the horizontal loading of ground motion as shown in Fig. 2. This is achieved through introducing an interface with relatively low horizontal stiffness between the foundation and the base of the superstructure. This interfacing element is the so-called base isolation system. The main purpose of the isolation system is to increase the natural period of a rigid structure (usually possesses very short first mode period). Thus, it makes it possible for a structure with very much lower fundamental frequency as compared to fixed-base frequency and also the predominant frequencies of the ground motion.

The main principle of seismic isolation is to prolong the period of the isolated structure. Logically, it works effectively for short structures as their period is usually very small, typically less than 1 second. Meanwhile, the natural period increases with increment of the structure's height. For very tall structure where the natural period is long enough to attract low earthquake forces, seismic isolation is considered redundant.

The second school of thought regarding seismic base isolation is the reduction of seismic force demand through providing additional damping capability to the vibrating system, besides prolonging the fundamental period. In linear equivalent static analysis of base isolation system using the constant velocity approach, the reduction of spectra acceleration and displacement is apparent when damping ratio increases (Fig. 3). In many earthquake prone countries, the design codes required at least 24 % of critical damping to be used in base isolation system (Kelly 2001; Abrishambaf and Ozay 2010; Kubin *et al* 2012; Danila 2013; Danila *et al* 2014). According to EN15129 (CEN 2007), elastomeric rubber bearing possessing damping ratio above 6 % is deemed as high damping rubber bearing (HDRB), and typical damping of HDRB is in the range of 8 to 12 percent depending on the shear modulus of rubber compound used. This leads to development of lead rubber bearing and other mechanical damping devices to go along with HDRB which not only causes very expensive base isolation system but to some extend compromising the durability and strength of rubber compound by altering the vulcanization process to increase the damping ratio which is widely practiced in the industry.

2. Literature review

Numerous researches of seismic isolation using HDRB have been carried out by many researchers particularly by in earthquake prone countries. Most of these studies (Kikuchi and Aiken 1997, Chung *et* al 1999, Wu and Samali 2002, Moroni *et* al 2006, Falborski and Jankowski 2012), used scaled-down HDRB due to shake table limitations, while individually isolated HDRB tests were performed by the manufacturers merely for quality control purpose (Malek *et al* 2012). Design and performance of demonstration building with high damping rubber bearings can be found in Ahmadi *et al* (1995). The paper described in detail the design and construction of the high damping rubber bearing for a four storeys low-cost housing in Indonesia. Taniwangsa (2002) presented the similar approach for a demonstration building in Lahad Datu, Malaysia. Braga and Laterza (2004) also performed field testing of a four-storey base isolated building excited by on-site actuator.

Up to 2010, there are approximately 10,000 buildings around the world that are seismically isolated (Forni 2010). Among the ten thousand buildings, most of them are installed with HRDB. Nevertheless, being deemed as expensive anti-seismic approach (Sayani 2009), the concept of HDRB is only used in providing seismic isolation in large, expensive and important structures such as museum, hospital, and etc. Very few low rise buildings in the range of light-to-medium weight are installed with HDRB due to economic purpose (Thurston 2006).

In most base isolation structures, the superstructures were relatively heavy (Forni 2010) and the design of HDRB for this kind of structure would produce higher safety factor compared to the lighter superstructure. Sarrazin (1992) reported that the cost of base isolation was approximately 25 % of total construction price. Such high initial capital has impeded usage of base isolation in lightweight structure as the reduction of cost was not apparent over the years. According to Sayani (2009), the total construction cost of base isolated structure was 10 % higher. While the cost of superstructure was reduced by 30 %, additional expenditure was required in foundation works and modified mechanical systems within the building. Since HCPS would be used ideally for low-rise residential housing or commercial shop-houses which would be relatively lighter compared to most base isolated structures such as towers, hospital buildings and bridges which were heavier in mass, the capability of the base isolator to meet required lateral displacement became questionable (Naeim and Kelly 1999). In other words, the HDRB becomes unstable when the imposed vertical load gets smaller if the designed lateral displacement remains the same.

The base isolation of lightweight structure was not addressed by previous study of small scale superstructure such as those investigated by Kikuchi and Aiken (1997). The target period of the base isolation system was near the corner period of response spectra due to the small vertical loading superstructure. Therefore, the HDRB provided less effective seismic isolation because of the high shear stiffness. The same phenomenon appeared in the study by Chung *et al* (1999). The designed elastomeric rubber bearing was unable to meet target isolation period beyond 2.0 s. The quarterly scaled rubber bearing was designed for 0.8 s while the actual prototype of full scale bearing was able to provide 1.6 s. The rubber bearing used by Wu and Samali (2002) too was having first natural period of 0.22 s. Therefore, the instability of HDRB in isolating lighter structure remains unanswered and there is not much published information available.

Studies on the effect of damping of base isolation system was not conclusive as many earthquake prone countries (particularly those in Asia and some Mediterranean states) still require high damping ratio (24 to 28 %) rubber bearing to be used. Kelly (1999) presented the coupled modal equations of motions when higher damping was introduced into the base isolation system. As a result, the higher mode response was increased and this led to increased floor acceleration despite reduction in base shear and displacement. Yoo and Kim (2002) investigated the performance of increased damping of lead rubber bearing (LRB) while Politopoulos (2008) studied the uncoupled equations of motions of the second mode of a 2 degree-of-freedom simplified system. The latter study suggested that while increasing hysteresis damping of isolation system decreased the base shear, displacement and acceleration demand of the first mode response, amplification of these values were observed particularly in floor acceleration response in higher mode frequencies.

Therefore, this paper investigated the seismic performance of base-isolated lightweight structure under various vertical loading excited with different classifications of *a/v* ground motion record (Zhu *et al* 1988, NBCC 1985, Elnashai and Mcclure 1996). The effect of different HDRB damping ratio (i.e. β = 8% and 24%) was also included.

3. Research methodology

3.1 Superstructure

The superstructure to be base-isolated seismically in this study was an innovated precast concrete wall system (HC Precast System or in short, HCPS) which was widely used in low-rise buildings (Tiong *et al* 2013). In general, the dimension and major reinforcement bars of the two stories precast wall building are shown in Fig. 4. Three types of vertical loading were considered in the seismic analyses, considering the different possible structural configuration and loading requirement as shown in Fig. 5 and Table 1. The dead load (DL) was taken from the self-weight of the structural elements themselves while live load (LL) was obtained from BS 6399: Part 1 (1996). HCPS-VL1 consisted of possible minimum loading that may be imposed on the structure while HCPS-VL3 comprised the probable maximum loading. The intermediate vertical loading which represented typical weight carried by many shophouse structural layouts was denoted by HCPS-VL2. The maximum intensity of distributed load for LL was taken as the maximum probable loading 4.0 kN/m^2 due to the wide range of possibility of commercial shop lot usage while the minimum one was 1.5kN/m^2.

Table 1 Three different configurations of HCPS with different imposed vertical loads

	HCPS-VL1	HCPS-VL2	HCPS-VL3
Wall type	Exterior	Interior	Interior
Slab length	3.5m	8.0m	8.0m
Nos. of storey	2	2	2
Live load	1.5 kN/m^2	1.5 kN/m^2	7.0 kN/m^2
Total weight	265 kN	995 kN	1475 kN

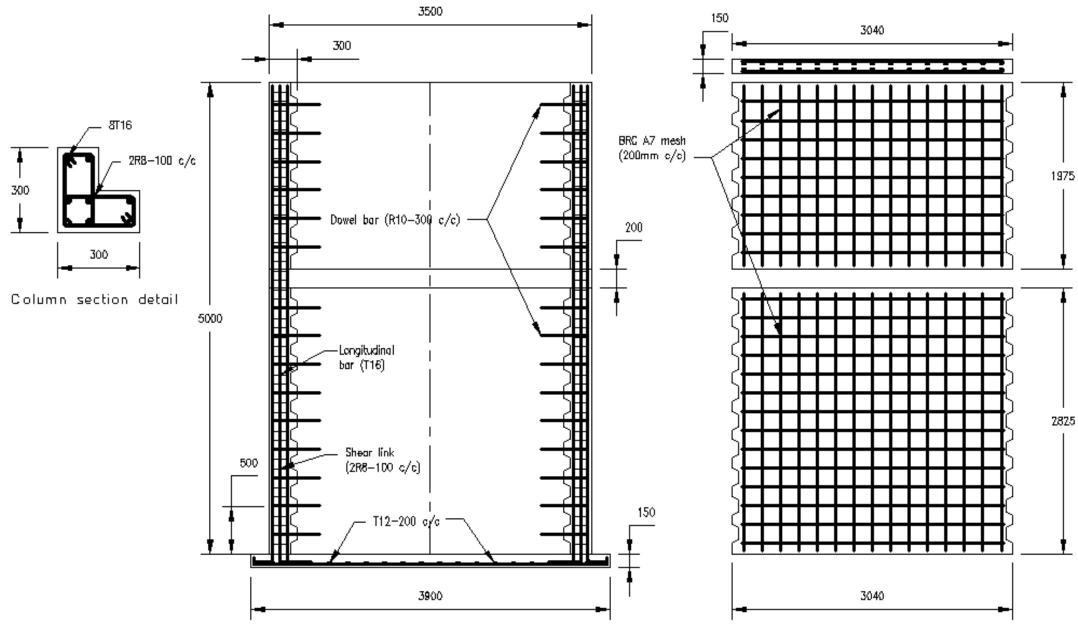

Fig. 4 Structural detailing of HCPS

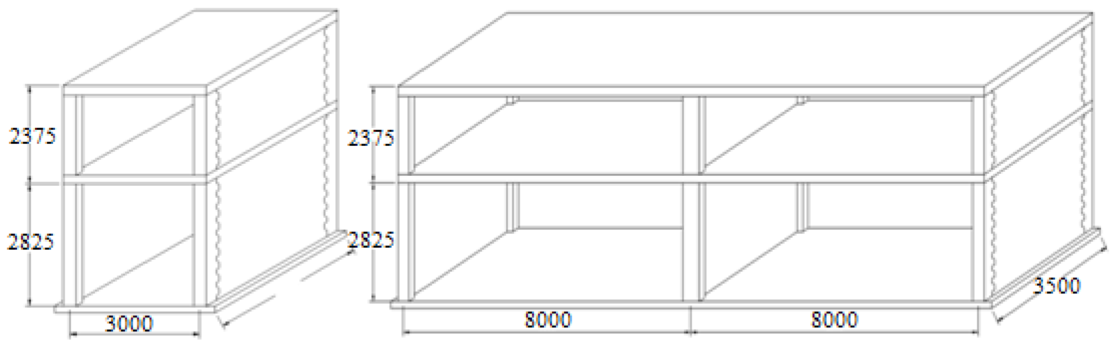

Fig. 5 (a) HCPS-VL1 and (b) HCPS-VL2 and HCPS-VL3

3.2 Property of high damping rubber bearing (HDRB)

This subsection presents the design and manufacturing process of the high damping rubber bearings (HDRB) used in this study. Three types of HDRB were designed respectively based on the different vertical loadings from superstructures, each for HCPS-VL1, HPCS-VL2 and HCPS-VL3. The naming convention of the HDRB is listed in Table 2. The design of HDRB was based on the approach found in Naeim and Kelly (1999). The initial step was to select target design period T_D of the base isolated structure. Typically, the design period was in the range of 2 to 3 seconds. In this study, the base isolated period of HCPS was targeted to be 2.5s. From the selected target period, the design outputs of all three HDRB are listed in Table 3.

Unplugged hole was provided in the middle of all three HDRB for two reasons. Firstly is to provide workability during manufacturing process of the rubber bearings (at least this was the case for HDRB-VL2 and HDRB-VL3). However, the hollow section was provided in HDRB-VL1 to reduce the loaded area while maintaining the plan dimensions as permitted in BS EN1337-3 section 5.3.2 (CEN 2005). This was essential in order to keep the design shear strain below 150 % while satisfying rollout requirement. Otherwise, the bearing would be too slender to facilitate the same target period of 2.5 s for HCPS-VL1. There is no clear guideline of the limitation in providing uniform holes within a particular elastomeric rubber bearing. However, the presence of hollow section changed the calculation of compression modulus E_c by adding in an additional reduction factor λ as shown in Eq. (1). Nevertheless, all three types of HDRB were checked to ensure that the designed sections satisfied the safety factor *SF*, rollout stability and compression limit. Briefly, *SF* refers to the ratio of buckling load to the designed compressive loading. Therefore, lower *SF* indicates higher potential for buckling when the designed vertical load is imposed onto it.

$$\lambda = \frac{b^2 + a^2 - [(b^2 - a^2)/\ln b/a]}{(b-a)^2} \tag{1}$$

where *a* and *b* are the inside and outside radius respectively.

Table 2 Naming convention of the HRDB used in this study

Bearing type	Superstructure	Bearing name
1	HCPS-VL1	HDRB-VL1
2	HCPS-VL2	HDRB-VL2
3	HCPS-VL3	HDRB-VL3

Table 3 Detail of high damping rubber bearing (HDRB) used in this study

Parameter	Unit	HDRB-VL1	HDRB-VL2	HDRB-VL3
Design vertical load	kN	65	250	365
T_D	s	2.5	2.5	2.5
$\emptyset_o$	mm	180	250	290
$\emptyset_i$	mm	90	50	50
t_r	mm	110	110	110
h_t	mm	160	146	138
n	nos.	26	19	15
t	mm	4.23	5.79	7.33
n_s	nos.	25	18	14
t_s	mm	2	2	2
K_H	N/mm	63.6	171.4	233.1
K_V	N/mm	52932.9	187120.0	225531.3
SF	-	2.7	3.3	3.3
D_D	mm	150	150	150
Expected ζ	%	8	8	8

Where T_D= design period, $\emptyset_o$ = outside radius, $\emptyset_i$= inside radius, t_r= total elastomer (rubber) thickness, h_t= total height of rubber bearing, *n* = quantity of rubber layer, *t* = thickness of each rubber layer, n_s= quantity of steel shim layer, t_s= thickness of steel shim, K_H= shear stiffness, K_V= compression stiffness, D_D=design displacement and ζ = expected critical damping ratio

All three HDRB-VL1, HDRB-VL2 and HDRB-VL3 were tested for compression stiffness (K_V) and lateral stiffness (K_H) according to the testing specifications listed in EN15129 (CEN 2007). In compression stiffness test, the HDRB was subjected to vertical compression loading increment until the design vertical (axial) load was reached, followed by unloading until zero load point. Such process was repeated for three cycles, and the compression stiffness was measured from the third cycle. Fig. 6 shows the compression stiffness testing setup for the three HDRB.

Interestingly, HDRB-VL1 failed in the compression test. Although it possessed the lowest safety factor *SF* against buckling of 2.7 compared to the two other HDRB with *SF* of 3.2, all design requirements and checking suggested that the design of HDRB-VL1 to be adequate. Fig. 7 presents the compression stiffness test results of HDRB-VL1. Initial compression witnessed linear vertical stiffness until the vertical displacement reached approximately 21 mm although the bearing started to be in twisted condition. However, the subsequent unloading had witnessed strain-hardening within the rubber bearing where larger decompression force was required to reduce the vertical displacement for next cyclical loading. Nevertheless, the compressive cyclic load-deformation exhibited highly nonlinear-elastic relationship despite the bearing actually suffered physical failure**.** Fig. 8 shows the failure of the cross section obtained by cutting through the HDRB after the compression test. Examining the cross-sectional cut, failure occurred within the internal diameter at the hollow section. The high concentration of compressive stress caused the rubber to twist, forcing the steel plates to buckle in its weaker axis. Combination of the whole failure mechanism had forced the HDRB to twist in its weakest axis. Therefore, it should be noted that extra precaution should be taken into consideration when providing hollow opening within the HDRB. The vertical stiffness of HDRB-VL2 and HDRB-VL3 in comparison to the estimated design values are shown in Table 4.

As shown in Table 4, huge difference occurred between the estimated vertical stiffness and those obtained from laboratory test results. One main reason for such phenomenon was due to the higher compressibility of rubber property particularly. In design calculation of HDRB, the value of rubber bulk modulus *K* ranged from 1000 MPa to 2500 MPa and it was difficult to be quantified (Naeim and Kelly, 1999). Thus, in practice, K is often taken as 2000 MPa.

Test setups of all three HDRB in single shear configuration are shown in Fig. 9. The HDRB was loaded with design vertical loading except for HDRB-VL1, and then forced to displace in the lateral direction simultaneously to reach design shear strain γ of 1.5. The lateral loading-unloading

Table 4 Designed vertical stiffness compared to laboratory results

	Designed (K_V) (kN/mm)	Laboratory obtained (K_V) (kN/mm)
HDRB-VL1	52.932	N.A. (failed in compression test)
HDRB-VL2	187.120	35.317
HDRB-VL3	225.531	54.176

Table 5 Designed shear stiffness and expected damping ratio compared to laboratory test results

	Designed values		Laboratory results	
	K_{eff} (kN/mm)	β (%)	K_{eff} (kN/mm)	β (%)
HDRB-VL1	0.064	8.0	0.072	9.5
HDRB-VL2	0.171	8.0	0.174	8.6
HDRB-VL3	0.233	8.0	0.229	8.0

was controlled at 0.4 Hz, or 2.5 s corresponding to the design period of the isolation system for four complete cycles. Results of the hysteresis loops are shown in Figs. 10-12 and the interested parameters such as effective lateral stiffness, initial stiffness, post-yield stiffness, vertical stiffness and hysteresis damping factor were taken on the third cycle. Comparison between the designed shear stiffness and those obtained from laboratory test results are shown in Table 5.

Unlike compression stiffness, the laboratory test results obtained for lateral shear stiffness and damping factor were in good agreement to the designed values. This was mainly due to the design of HDRB using directly the shear modulus value (*G*) while the compressive modulus value (E_c) was a function of shear modulus (*G*), shape factor (*SF*) and bulk modulus (*K*).

3.3 Time history analysis

The HDRB was located beneath the column for both structural configurations as shown in Fig. 13. Two different methods were used to calculate the linear shear stiffness K_1 and post-yield stiffness K_2 of HDRB respectively. This study adopted the method proposed by Naeim and Kelly (1999) in which the linear shear stiffness K_1 was obtained from the hysteresis loops by the best fit function of initial slope during the unloading cycle. As it was difficult or almost impossible to obtain the value of K_1 n the initial loading phase due to large internal resistance of both the mechanical actuator system and rubber compound, K_1 was obtained from the unloading slope. Meanwhile, the value of post-yield stiffness K_2 was calculated using Eq. (2) according to EN 15129.

$$K_2 = \frac{F(d^+) - F(d^+/2)}{d^+} - \frac{F(d^-/2) - F(d^-)}{d^-} \tag{2}$$

where $\mathrm{F}^+, \mathrm{F}^-$ refer to maximum and minimum horizontal forces observed in the complete loading-unloading cycle while $\mathrm{d}^+, \mathrm{d}^1$ are the corresponding lateral displacements.

The main frame of HCPS consists of reinforced concrete columns, slabs as well as precast concrete wall panels. The columns were modeled using frame element, with reinforcement details found in Fig. 4. The precast wall panel was modeled using nonlinear (layered) shell element. The material angle of the mesh reinforcement (BRC A7) was assigned material angle of 0^0 (for horizontal rebar) and 90^0 for vertical rebar to align it with the shell local-2 axis.

The proposed FE model resolved into detail the interface made by shear key and dowel bar into basic reaction forces, as shown in Fig. 14. The shear key protruded along the height of column would mainly be taking all gravitational (vertical) loading from the wall panel. This was represented by a rotational spring element with highly rigid moment-rotation behaviour. Next, the dowel action was assumed to be responsible for resisting all tensile pulling force between the wall and column. Hence, a translational nonlinear link (without having any rotational capability) was assigned to represent the dowel actions. The maximum pullout force (anchorage) of dowel bar was estimated using Eq. (3) while the deformation of normal rebar under tensile stress was based on Bljuger (1988). The plastic behaviour of dowel reaction was represented by means of the force-deformation relationships based on the bi-linear model (Fig. 15). Considering that upon reaching maximum pullout capacity, the dowel bar has very minimal residual strength to resist further tensile force; a sudden drop of strength (130 kN/mm) was assigned as the post-yield stiffness. Another nonlinear link element was also introduced to represent the shear key contact surface or interface between the precast panel and column members. While this surface would purely be attributed to plain concrete, the weak tensile strength of the concrete was modeled assigning hook element and the compressive strength of concrete shear key included potential shear failure of the element (Soudki *et al*. 1996). The ultimate concrete tensile and crushing (or failure in shear) stress was converted into maximum permissible force by multiplying the area of shear key in contact.

$$V = 0.6F_b \tan \alpha_f \tag{3}$$

where V = ultimate pullout force; F_b = anchorage values of reinforcement; α_f = internal friction between the interfaces

Hysteresis loops of base shear response versus top displacement of HCPS (obtained from both experimental work and FE model) are shown in Fig. 16. In general, the hysteresis behaviour between the experimental results and FE model were in good agreement. Detailed discussion of the results can be found in Tiong *et al* (2013). Besides the lateral quasi-static test, a 1:3 HCPS test model was constructed and tested on shake table to obtain both natural period and seismic responses. Predominant natural period (first mode) of the scaled-down model was obtained in experimental using white noise excitation by the shake table. Both experimental and FE model had predicted the first natural period of 0.012 s. As it was not the scope of this paper to discuss in detail the scaled-down test, more information of the shake table test can be found in Tiong (2014).

(a) HDRB-VL1

(b) HDRB-VL2

(c) HDRB-VL3

Fig. 6 Compression stiffness test of the three HDRB under designed loads

Table 6 Value of K_1 and K_2 used for base isolation element in FE model

Bearing Type	K_1 (kN/mm)	K_2 (kN/mm)
HDRB-VL2	0.703	0.147
HDRB-VL3	1.321	0.277

Table 7 Details of selected ground motion for time history analysis

#EQ	Earthquake Name	Direction	Year	Station Name	Fault Type	*a/v* (g/ms^{-1})	Distance (km)
1	Kocaeli, Turkey	180^0	1999	Bornova	SS	0.48	275
2	Kocaeli, Turkey	90^0	1999	Bornova	SS	0.42	275
3	Kocaeli, Turkey	0^0	1999	Manisa	SS	0.4	660
4	Kocaeli, Turkey	90^0	1999	Manisa	SS	0.22	660
5	Imperial Valley-06	0^0	1979	El Centro Array #7	SS	0.75	211
6	Imperial Valley-06	90^0	1979	El Centro Array #7	SS	0.82	211
7	Loma Prieta	140^0	1989	Foster City - APEEL 1	RV-OBL	0.33	116
8	Loma Prieta	230^0	1989	Foster City - APEEL 1	RV-OBL	0.45	116
9	San Fernando	0^0	1971	Cholame	RV	1.67	185
10	San Fernando	90^0	1971	Cholame	RV	1.50	185
11	San Fernando	135^0	1971	Borrego Springs	RV	2.67	271
12	San Fernando	225^0	1971	Borrego Springs	RV	2.67	271
13	Chi-Chi, Taiwan-03	231^0	1999	TCU085	RV	1.40	1000
14	Chi-Chi, Taiwan-03	51^0	1999	TCU085	RV	1.25	1000
15	Little Skull Mtn,NV	East	1992	Station #6-Las Vegas	N	0.51	660
16	Little Skull Mtn,NV	North	1992	Station #6-Las Vegas	N	0.48	660
17	Little Skull Mtn,NV	0^0	1992	Station #7-Las Vegas	N	0.63	275
18	Little Skull Mtn,NV	270^0	1992	Station #7-Las Vegas	N	0.63	275
19	Chi-Chi, Taiwan	0^0	1999	KAU011	RV-OBL	0.92	155
20	Chi-Chi, Taiwan	270^0	1999	KAU011	RV-OBL	1.40	155
21	Irpinia, Italy-01	East	1980	Bagnoli Irpinio	N	1.17	1000
22	Irpinia, Italy-01	North	1980	Bagnoli Irpinio	N	1.06	1000
23	Northridge-01	0^0	1994	Pacoima Dam	RV	0.71	2016
24	Northridge-01	270^0	1994	Pacoima Dam	RV	0.42	2016
25	Loma Prieta	175^0	1989	Corralitos	RV-OBL	1.05	462
26	Loma Prieta	265^0	1989	Corralitos	RV-OBL	0.64	462
27	Kobe, Japan	90^0	1995	0 Kakogawa	SS	1.25	22.5
28	Tabas, Iran	0^0	1978	71 Ferdows	RV	1.26	91
29	New Zealand	353^0	1987	Matahina Dam	N	1.08	16.1
30	Malaysia (Artificial)	NA	NA	NA	NA	2.84	400
31	Irpinia, Italy	270^0	1980	Bagnoli Irpino	N	0.63	8.2
32	Duzce, Turkey	300^0	1999	Ambarli	SS	0.51	189
33	SMART1, Taiwan	North	1983	28 SMART1 M01	RV	0.78	27.4

Fault type: SS = strike slip; RV = reverse; RV-OBL = reverse oblique; N = normal; NA = not applicable

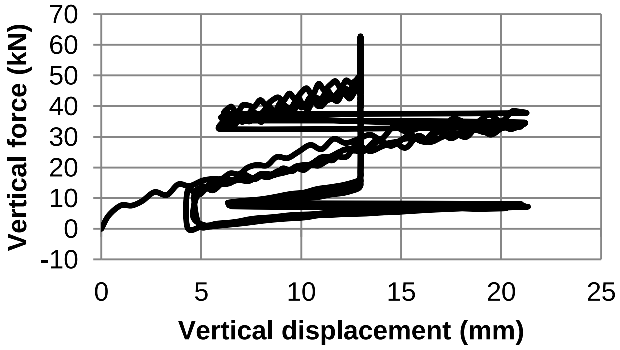

Fig. 7 Compression stiffness test result of HDRB-VL1

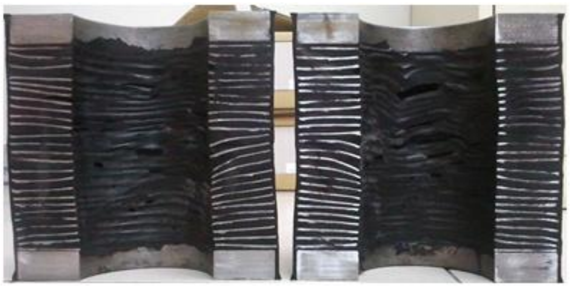

Fig. 8 Cross-sectional cut of HDRB-VL1 revealing bending of steel plates

(a) HDRB-VL1 (b) HDRB-VL2

(c) HDRB-VL3

Fig. 9 Shear stiffness testing configuration of the three HDRB to $\gamma = 150$ %

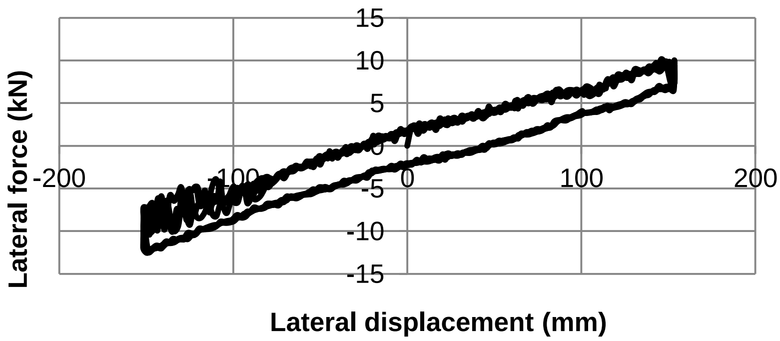

Fig. 10 Hysteresis loops of shear stiffness test for HDRB-VL1

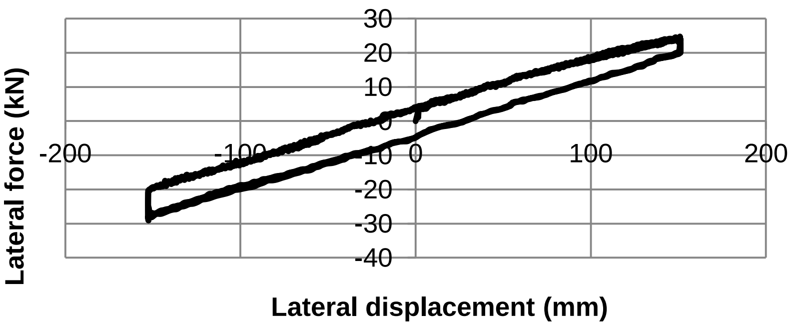

Fig. 11 Hysteresis loops of shear stiffness test for HDRB-VL2

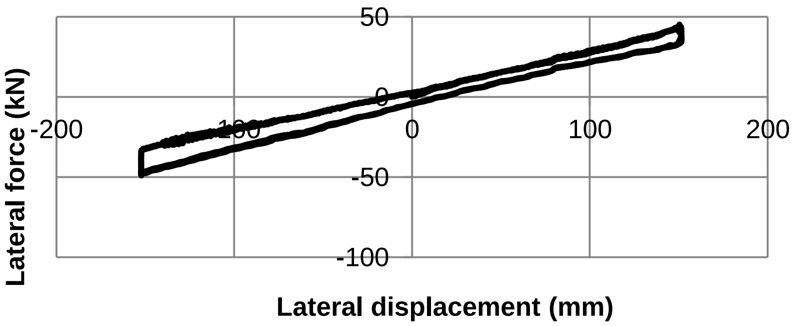

Fig. 12 Hysteresis loops of shear stiffness test for HDRB-VL3

The damping of the base isolated superstructure was assumed to be 2 % of critical damping as recommended by Chopra (2007), not the typical 5 % used in conventional fixed base structural analysis. As base isolated building should not be expected to suffer non-structural damage, a lower damping value is appropriate. Stiffness of the HDRB (modeled by isolator element) is listed in Table 6.

A total of 33 time histories of real earthquake records were used in the time history analysis of the base isolated structure. Summary of the selected ground motion data is listed in Table 7. The direction of earthquake in Table 7 was measured in terms of degree (^{0}) from North to the

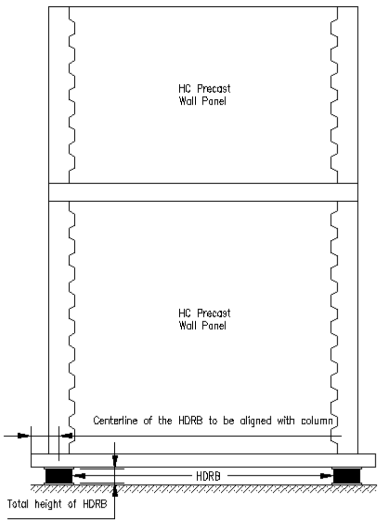

Fig. 13 Location of HDRB beneath the precast wall system

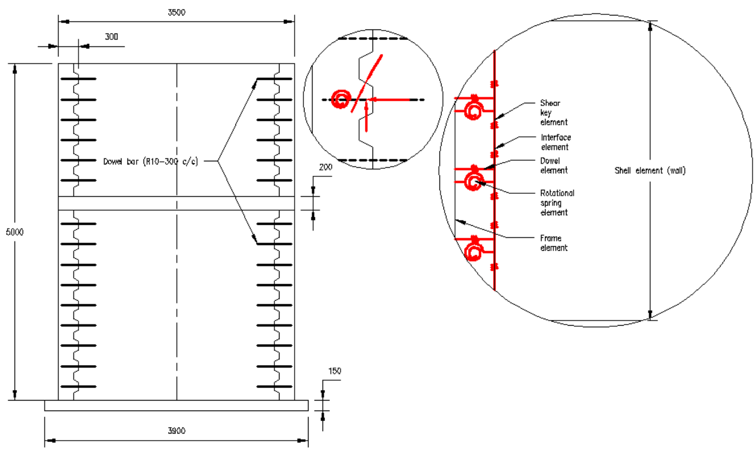

Fig. 14 Assigned nonlinear elements in FE model to represent wall-column interfaces

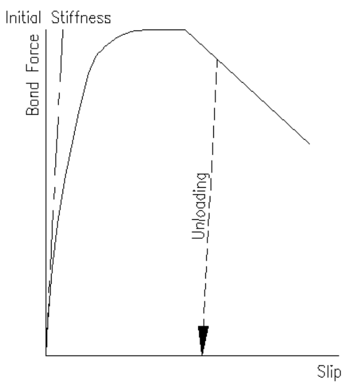

Fig. 15 Hysteresis model for dowel actions (Hashemi et al 2009)

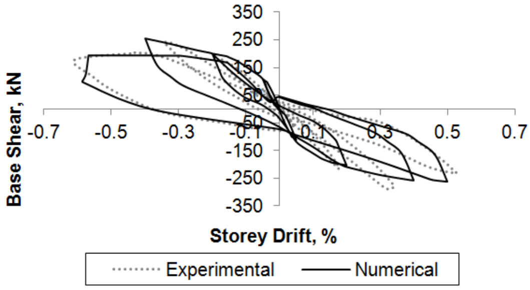

Fig. 16 Hysteresis curves of HCPS from experimental and FE model

orientation of the sensor component in clockwise direction. The earthquake records were carefully selected to cover a wide range of parameters such as distance from recording station to epicenter, soil condition, magnitude and fault type. Most importantly, the peak ground acceleration to peak velocity ratios (*a/v*) of all 33 time histories were used to classify the ground motion intensity (Elnashai and Mcclure 1996). According to Zhu *et al* (1988), earthquake ground motions are divided into three categories as follow:

(a) Normal ground motions possessing significant energy over a broad frequency range
(b) Ground motions that are rich in large amplitude with high frequency vibrations
(c) Ground motions that possess energy contained in long period waves

The peak ground acceleration to peak ground velocity (*a/v*) ratio was proposed by Zhu *et al* (1988) to represent the three categories of earthquake ground motions. Because peak accelerations are associated with low period excitations while peak ground velocities are related to moderate to low frequency oscillations, a large *a/v* ratio indicated type (b) earthquakes and type (c) ground motions will have lower *a/v* ratio. Based on the National Building Code of Canada (NBCC 1985), three categories of *a/v* ratios were considered in this study. Class 1 *a/v* are ground motions with *a/v* ratio smaller than 0.8 g/ms^{-1} while Class 3 *a/v* are earthquakes with *a/v* values larger than 1.2 g/ms^{-1}. Class 2 *a/v* are ground motions in between Class 1 and Class 3.

4. Results and discussion

The interested results obtained from the time history analyses would be the base shear and floor acceleration values of base isolated HCPS, namely the HDRB-VL2 and HDRB-VL3 in comparison to those values obtained from corresponding fixed base structures. From the same earthquake records, values of base shear and floor acceleration were obtained in both maximum and minimum (absolute) values.

4.1 Effect of a/v ratio of ground motion on seismic base isolation

Amplification of base shear responses for HDRB-VL2 ranged from 29 % in #EQ32 to 270 % by #EQ13. The amplification is shown as negative value (in terms of base shear reduction) in Fig. 17 since the reduction was calculated using Eq. (4). Compared to HDRB-VL2, the base shear amplification of HDRB-VL3 which ranged from 14% in #EQ1 to 131% in #EQ22 was lower than the former. Despite having reduced base shear responses by HDRB-VL2 in #EQ21, #EQ22, #EQ23, #EQ24, #EQ7 and #EQ8, amplification of base shear was observed in other remaining Class 1 *a/v* excitations Similar observations were also calculated from HDRB-VL3 responses.

$$\text{Base shear reduction (\%)} = \frac{\text{Base shear (HCPS) - Base shear (HDRB)}}{\text{Base shear (HCPS)}} \times 100\% \tag{4}$$

Amplification of base shear values were observed in most of the time history cases in low (Class 1) *a/v* base excitations. In HDRB-VL2, instead of reducing the base shear, 50 % of the 16 base shear values had shown amplification when the structure was base-isolated. Increment of gravity load carried by the structure which increased the mass of the isolated system as HDRB-VL3 revealed 63 % of the 16 base shear values were larger than the corresponding fixed-base structures. Although more earthquake records in the analysis of HDRB-VL3 showed amplification of base shear demand, it was observed that heavier mass of isolated superstructure led to smaller base shear amplification in this low *a/v* earthquake range. This was because the base shear of fixed base structure, HCPS-VL3 was larger than HCPS-VL2. Thus, when comparing the base shear of isolated system, HDRB-VL3 to HCPS-VL3, the amplification seemed to be smaller than HDRB-VL2. In other words, the reduction of base shear observed in HDRB-VL2 was larger than HDRB-VL3 in particular #EQ7, #EQ8, #EQ10, and #EQ24.

As shown in Fig. 18, the base shear reductions obtained from Class 2 *a/v* ground excitations for HDRB-VL2 ranged between 12 to 93 %. Meanwhile, the base shear reduction for HDRB-VL3 ranged from 22 to 98 %. Unlike the responses observed in Class 1 *a/v* earthquake records, all results of HDRB-VL2 and HDRB-VL3 had shown significant reduction in base shear values with no exception. In other words, the base shear values of all base isolated structure were smaller than their corresponding fixed base structures. Base shear responses of HDRB-VL2 seemed to be always smaller than HDRB-VL3. Nevertheless when compared to their corresponding fixed base structures, the percentage of base shear reduction for all cases observed in HDRB-VL3 ranged from 22 to 98% were larger than the 12 to 92 % in HDRB-VL2, particularly in #EQ29 and #EQ33. In other words, the base shear reduction in heavier structure above isolation system was more effective than lighter structure. As the mass of superstructure increases, the base shear value being

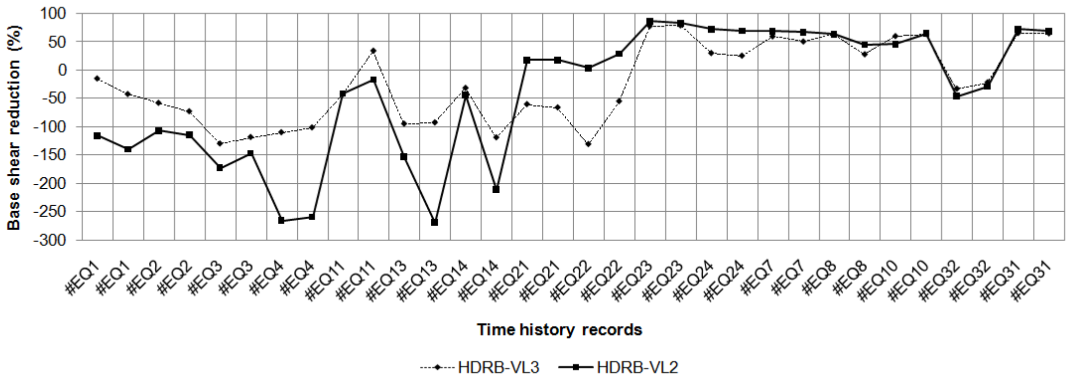

Fig. 17 Base shear reduction between HDRB-VL2 and HDRB-VL3 under Class 1 *a/v* ground motions

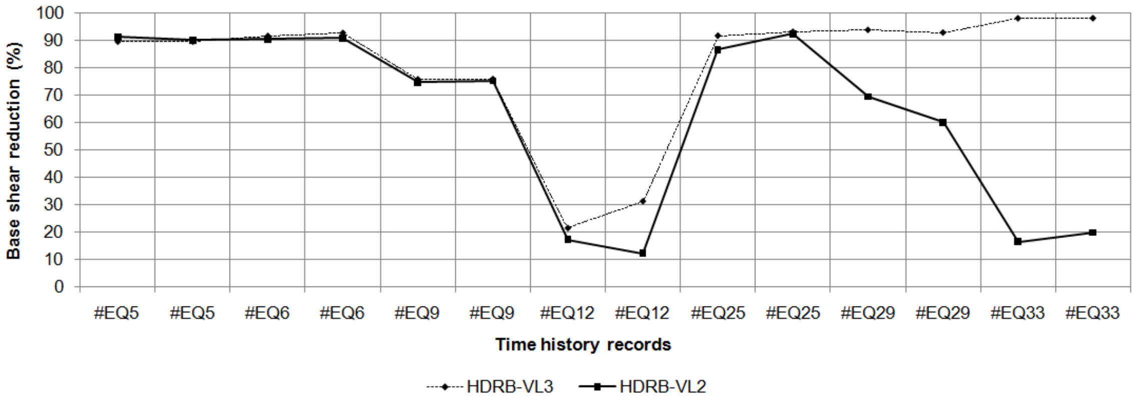

Fig. 18 Base shear reduction between HDRB-VL2 and HDRB-VL3 under Class 2 *a/v* ground motions

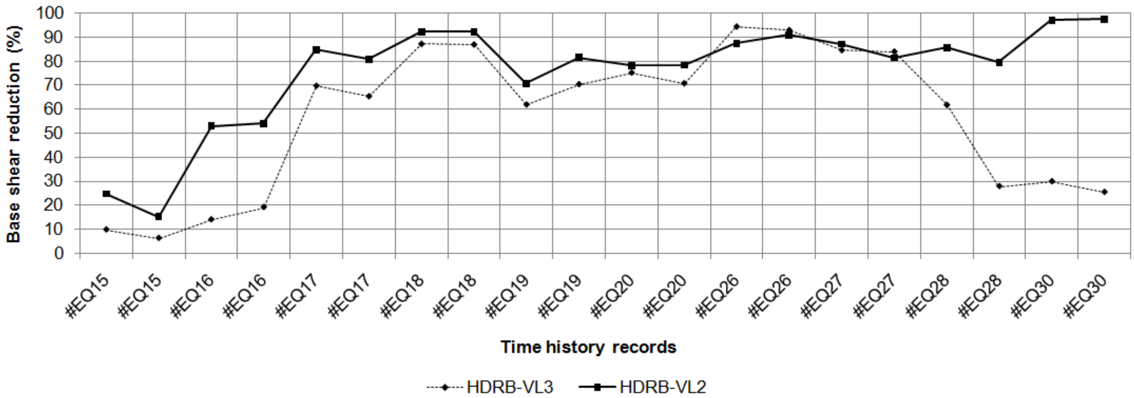

Fig. 19 Base shear reduction between HDRB-VL2 and HDRB-VL3 under Class 3 *a/v* ground motions

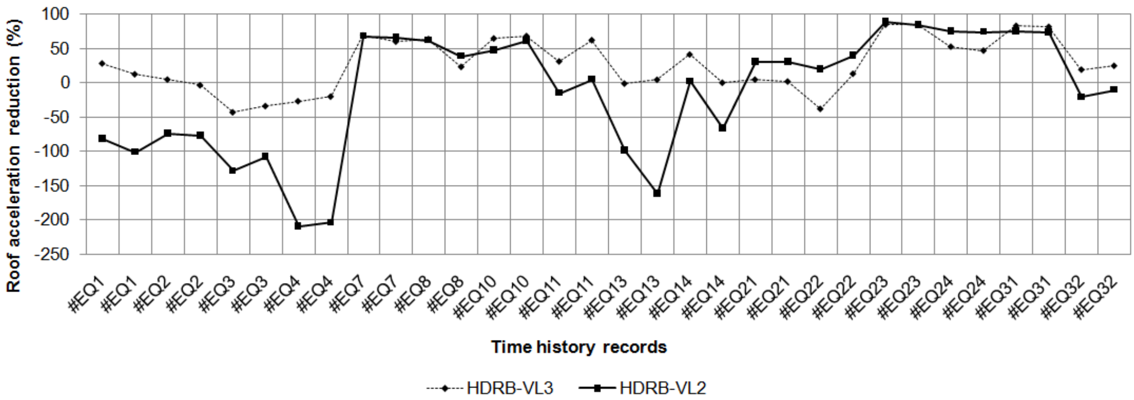

Fig. 20 Roof acceleration reductions of HDRB-VL2 and HDRB-VL3 in Class 1 *a/v* ground motions

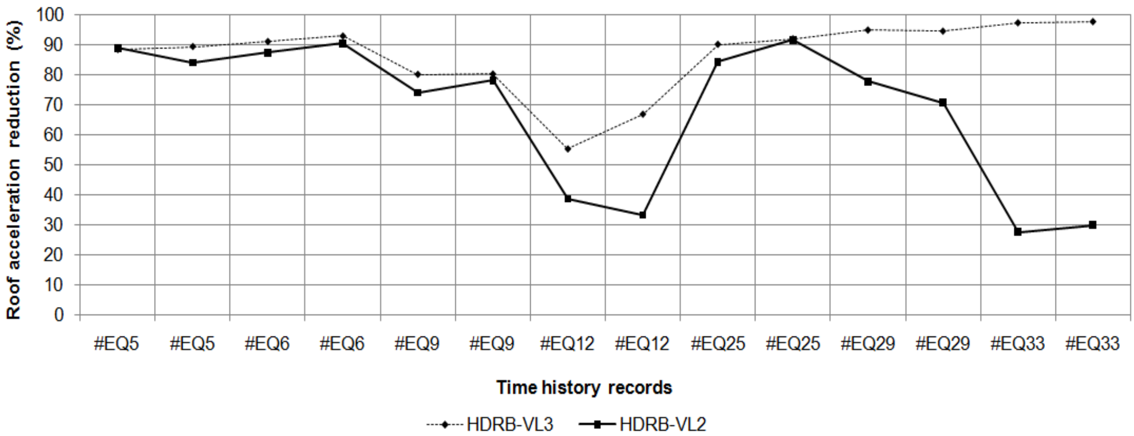

Fig. 21 Roof acceleration reduction of HDRB-VL2 and HDRB-VL3 in Class 2 *a/v* ground motions

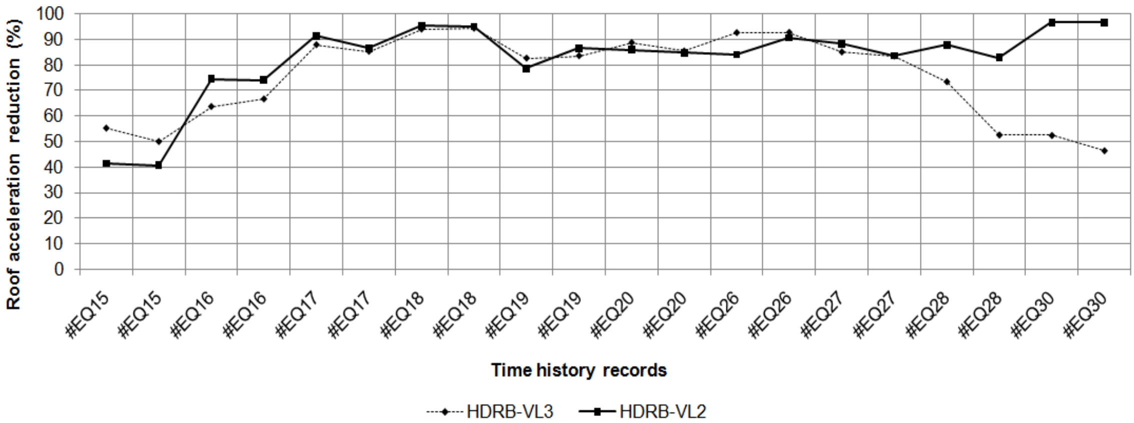

Fig. 22 Roof acceleration reduction of HDRB-VL2 and HDRB-VL3 in Class 3 *a/v* ground motions

proportionate to effective modal mass of fixed base structure increased vastly especially if the predominant period of the mass-increased structure was close to the peak of spectra. Consequently, prolonging the period through base isolation for heavier structure tended to reduce the base shear demand more drastically compared to lighter structure.

The base shear reduction of HDRB-VL2 ranged between 15 to 98 % in Class 3 *a/v* ground excitations. On the other hand, HDRB-VL3 revealed 6 to 95 % lower in base shear values compared to HCPS-VL3. Comparisons between the two reductions are shown in Fig. 19. Unlike Class 2 *a/v* earthquakes, base shear reduction in HDRB-VL2 was more significant than HDRB-VL3 under Class 3 *a/v* ground excitations. It showed that in very high seismicity area such as those recorded in this Class 3 *a/v* ground motions, providing base isolation to lightweight structure responded better in terms of base shear reduction. Therefore, higher *a/v* ratio of ground motion had shown significant effect on the base shear reduction capability of base isolation system with different superstructure mass. Such phenomenon was not observed in Class 2 *a/v* ground excitations.

Although large amplification of roof acceleration responses were observed in both HDRB-VL2 and HDRB-VL3, these amplified accelerations were considerably insignificant due to the fact that the fixed base values were too small; less than 19 gals for HDRB-VL2 and 15 gals for HDRB-VL3. In HDRB-VL2, 8 out of 16 time histories revealed amplification while only 3 time histories showed amplification in HDRB-VL3. Other remaining Class 1 *a/v* excitations revealed roof reduction between 2 to 85 % for both HDRB-VL2 and HDRB-VL3. It was observed that the base shear responses were orthogonal to roof acceleration particularly in HDRB-VL3 because the base shear was a function of mass while roof acceleration response was dependant on the targeted frequency of the base isolated system which remained the same in 2.5 s for both HDRB-VL2 and HDRB-VL3. Fig. 20 shows that the roof acceleration reduction of HDRB-VL3 was approximate to those of HDRB-VL2. However, in terms of amplification of the roof acceleration response, HDRB-VL2 possessed higher amplifying percentage with maximum of 210 % compared to HDRB-VL3 which only showed amplification up to 43 % in the Class 1 *a/v* ground motions.

In Class 2 *a/v* ground excitations, the range of reduction for HDRB-VL2 was 28 % to 92% while HDRB-VL3 recorded 56 to 97 % of fixed base values. The roof acceleration reduction was calculated similarly to the base shear reduction using Eq. (4) but this time, acceleration responses were used in the equation instead of base shear values. Roof acceleration reduction of HDRB-VL3 was more significant compared to HDRB-VL2 for all the seven time histories (Fig. 21). In this class of earthquake excitations, providing base isolation had managed to decrease the roof acceleration responses in both HDRB-VL2 and HDRB-VL3 vibrating system.

Fig. 22 shows the reduction of roof acceleration for HDRB-VL2 and HDRB-VL3 when excited with Class 3 *a/v* ground motions. The range of reduction for HDRB-VL2 was 41 % to 97 % while HDRB-VL3 showed 46 % to 94 % of fixed base values. In this class of earthquake records, the roof acceleration reduction of HDRB-VL3 could be considered to be approximately the same with HDRB-VL2 for at least 80 % of all 10 time history records. The roof acceleration reductions of both structures in Class 3 *a/v* ground motion were similar to those obtained in Class 2 *a/v*. In other words, the reduction of roof acceleration responses in base isolation system were independent to mass of the isolated structure and types of ground motion beyond Class 1 *a/v*.

In order to investigate the relationship between *a/v* ratio of ground motions on effectiveness of base isolation system, both the base shear and roof acceleration reduction of HDRB-VL2 and HRDB-VL3 are plotted against the ground motion *a/v* ratio in Fig. 23. It was observed from the figure that below *a/v* ratio of 0.5 g/ms^{-1}, the response of base isolated structure was complicated. While base shear and also roof acceleration were amplified in some cases, reduction up to 50 % was also noted in some cases within the similar *a/v* ratio. Therefore, structural engineers have to be extra careful when dealing with ground motion possessing this characteristic to ensure large amplification does not occur when base isolation is provided. However, providing base isolation system for structure located in seismic excitations with *a/v* ratio above $0.5g/ms^{-1}$ yielded significant reduction in both base shear and roof acceleration responses.

4.1.1 Effect of different damping ratio of base isolation system

In order to investigate the effect of providing base isolation system with higher damping ratio as recommended by engineering community in many earthquake prone regions, both characteristics of HDRB-VL2 and HDRB-VL3 were redesigned to possess at least 24 % damping ratio (β) as shown in Figs. 24 and 25 respectively. The effective shear stiffness ($\mathrm{K_{eff}}$) between the HDRB with 8 % damping and 24 % damping was kept identical.

Fig. 26 plots the ratio of base shear values for HDRV-VL2 isolated with rubber bearing having 8 % and 24 % damping factors using Class 1 *a/v* ground excitations. Similar plots for HDRB-VL2 obtained from Class 2 and Class 3 *a/v* earthquake records are shown in Figs. 27 and 28 correspondingly. The ratio of base shear is denoted by $\frac{V_{b8\%}}{V_{b24\%}}$. The dotted lines represent $\frac{V_{b8\%}}{V_{b24\%}} = 1$, meaning that the base shear values between the two base isolated systems are the same. Only 8 earthquake records, all from Class 1 *a/v* ground motions show reduction of base shear responses by 30% or 36 kN. Meanwhile, other remaining time histories indicate no significant reduction on base shear demand when applying base isolator with higher damping factor of 24 %.

In the remaining 25 time histories, the analysis of base shear demand revealed higher responses were obtained with the presence of 24% hysteresis damping as compared to the conventional 8 % natural rubber compound. It seemed that applying higher damping factor in Class 2 *a/v* excitations showed the least effective results with every ground excitation revealed amplification of base shear responses up to maximum of 58 %. On average, the rubber bearing with 8 % damping factor reduced the base shear responses by 3 %, 30 % and 23 % as compared to 24 % damped rubber bearing for Class 1, Class 2 and Class 3 *a/v* ground excitations respectively.

Such increase in base shear responses occurred due to the higher unloading stiffness of the rubber bearing of the 24 % damping. Although the effective stiffness of both 8 % and 24 % damping bearings were the same to achieve target period T_D of 2.5 s, the unloading stiffness of bearing with higher damping factor was 150 % stiffer than the 8 % damped rubber bearing. It was proven in the result that the stiffer unloading stiffness of the bearing was having more effect on the base shear demand to be compensated by the increment of hysteresis loop area or energy dissipation. Thus, the effect of higher modes became dominant and apparently, was unable to be reduced significantly by the additional damping factor provided through rubber bearing possessing larger hysteresis loop area.

Analysis of the roof acceleration responses revealed that only 6 time histories from the Class 1 *a/v* excitations showed significant reduction between 20 to 40 % of acceleration values in $\beta = 24\,\%$ bearing compared to the $\beta = 8\,\%$'s (Fig. 29). The roof acceleration responses of base isolated structure with 8 % damping factor was denoted by $a_{cc8\%}$ and for 24 % damping factor was $a_{cc24\%}$On average, the rubber bearing with 8 % damping factor surpassed the 24 % damping bearing in terms of roof acceleration responses by 3 %, 19 % and 13 % for Class 1, Class 2 (Fig. 30) and Class 3 *a/v* (Fig. 31) seismic ground excitations. In other words, increasing the damping ratio of base isolation interface did not improve the performance of base isolated system HDRB-VL2 in terms of roof acceleration reduction

When the mass of base isolated structure increased, the base shear demand in the Class 1 *a/v* excitations became complex (as revealed in the case of HDRB-VL3 which is shown in Fig. 32). It shows that 9 out of 16 time histories revealed that 24 % damping rubber bearing caused higher base shear values up to 60 % compared to the 8 % damping factor. On the other hand, 7 other remaining time histories showed significant reduction of base shear values of 110 % maximum by $\beta = 24\%$ rubber bearing.

The base shear reduction for HDRB-VL3 based on Class 2 *a/v* ground motions had an average of 9 % (Fig. 33). For Case 3 *a/v* excitations (Fig. 34), the average base shear reduction was 20 % if Kobe earthquake which biased heavily to 24 % damping factor was excluded. This could be the cause that leads to higher damping requirement stated by the Japanese, Turkish and Chinese earthquake committees. However, such demand based on earthquake with greater magnitudes could be rare, and it was revealed in this study that in most ground motions, the application of higher damping factor did not ensure satisfactory base shear or acceleration response reduction particularly in the region of Class 2, and 3 *a/v* ground excitations.

Based on the analysis results for Class 1 *a/v* seismic records shown in Fig. 35, 9 time histories had larger roof acceleration reduction in $\beta = 8\%$ over $\beta = 24\%$ with maximum reduction up to 55 %. However, the remaining 7 ground motions showed larger roof acceleration reduction by $\beta = 24\%$ up to 58 % compared to $\beta = 8\%$. For Class 2 *a/v* ground excitations (Fig. 36), almost all of the roof accelerations of $\beta = 8\%$ are lower than $\beta = 24\%$. The average reduction was 14 %.

The average roof acceleration reduction was 13 % for Class 3 *a/v* excitations (Fig. 37), excluding Kobe earthquake. Kobe earthquake record revealed lower roof acceleration in $\beta = 24\%$ over $\beta = 8\%$ by 66 %.

Relationship between ground motion *a/v* ratio on the effect of damping factor was complicated as shown in Fig. 38. In the range of *a/v* below 2g/ms^{-1}, the usage of higher damping factor might lead to larger reduction in some cases but amplification in others.

Providing higher damping ratio (e.g. β = 24 %) did not reveal positive reduction in both base shear demand and roof acceleration in many earthquake excitations used in this study especially when the mass of superstructure was lighter such as HCPS-VL2. Particularly in Class 2 and Class 3 *a/v* ground motions, amplification of seismic responses was observed in both HDRB-VL2 and

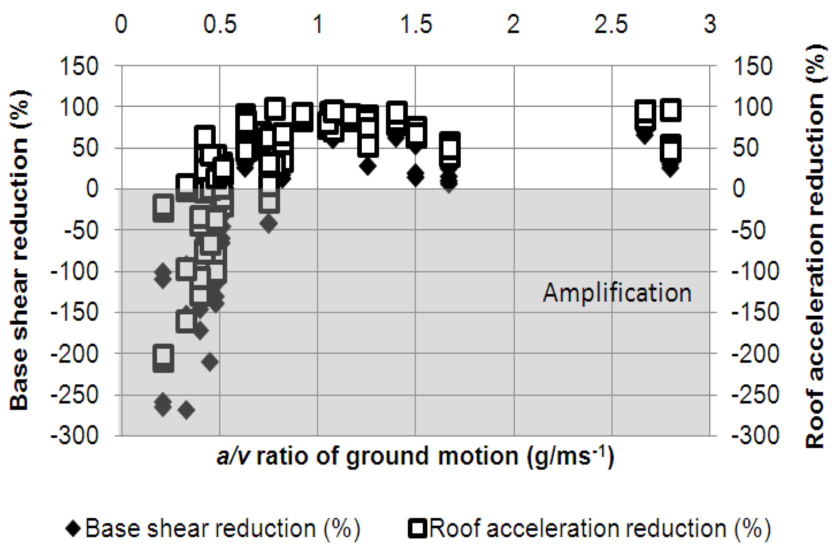

Fig. 23 Base shear and roof acceleration reduction versus *a/v* ratio of ground motion

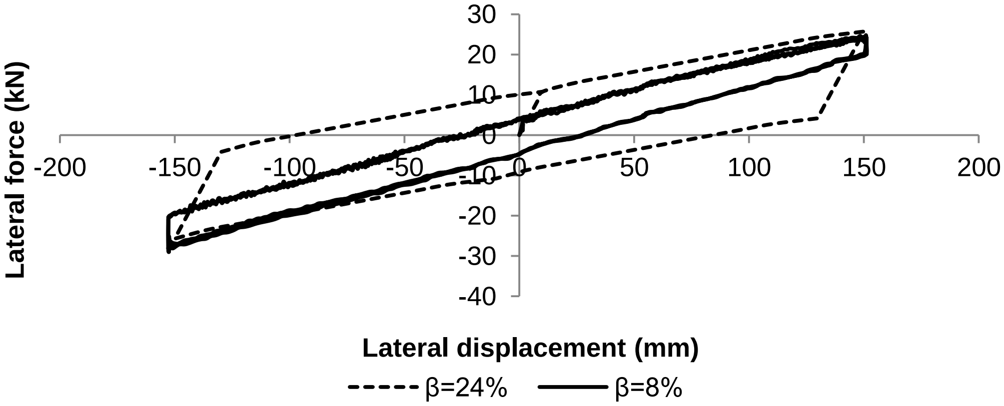

Fig. 24 Shear stiffness of HDRB-VL2 with β = 8% and 24%

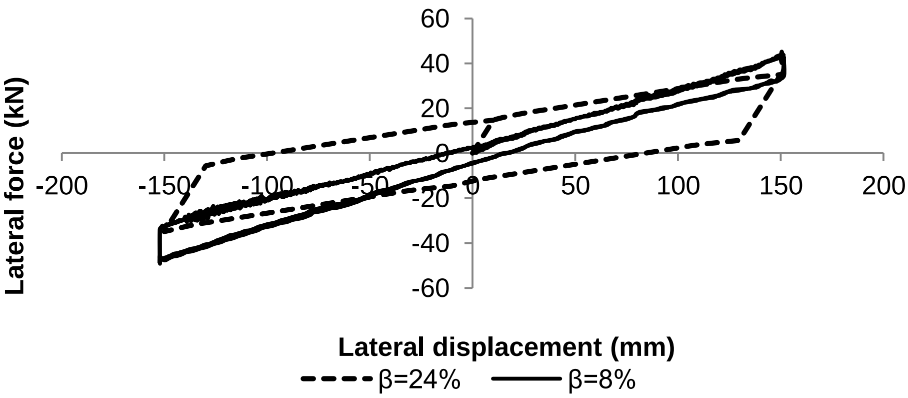

Fig. 25 Shear stiffness of HDRB-VL3 with β = 8% and 24%

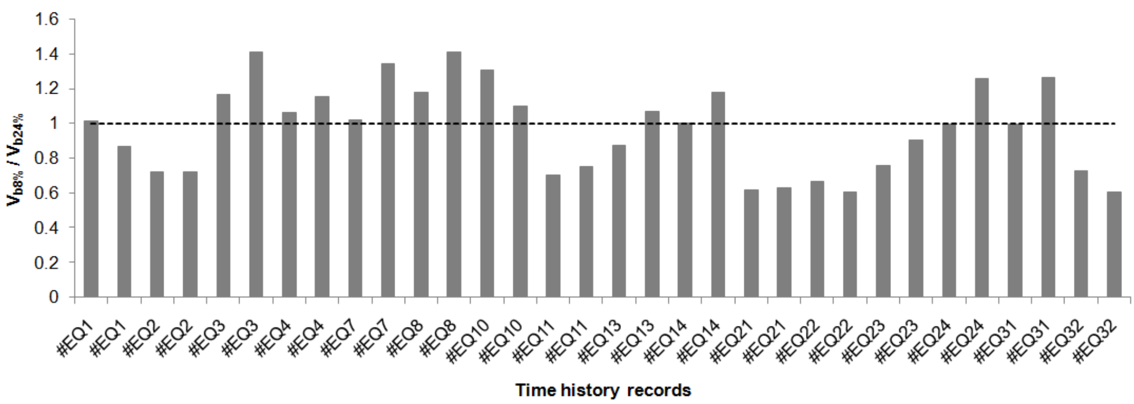

Fig. 26 Base shear ratio of HDRB-VL2 with β = 8 % and 24 % in Class 1 *a/v* ground motions

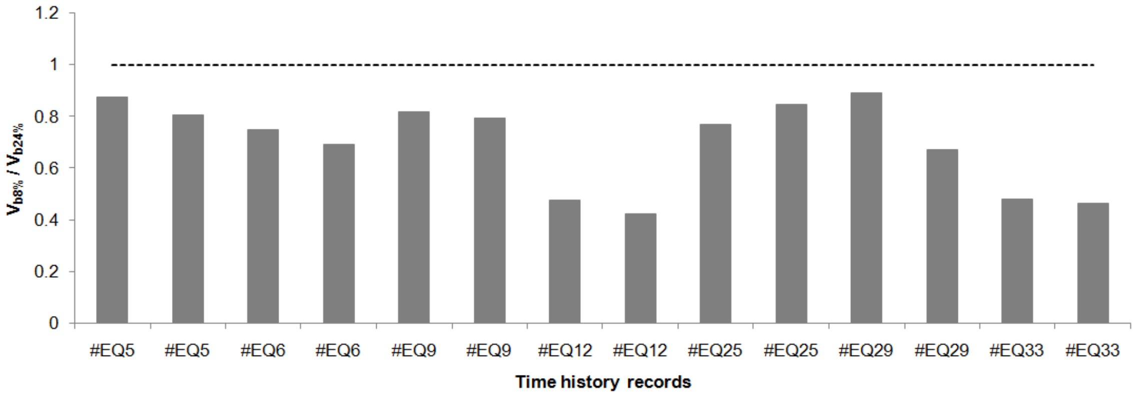

Fig. 27 Base shear ratio of HDRB-VL2 with β = 8 % and 24 % in Class 2 *a/v* ground motions

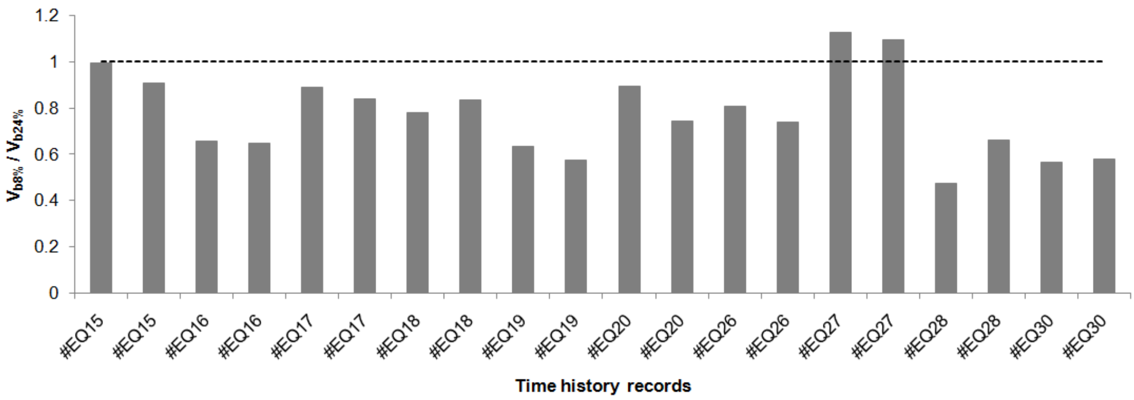

Fig. 28 Base shear ratio of HDRB-VL2 with β = 8 % and 24 % in Class 3 *a/v* ground motions

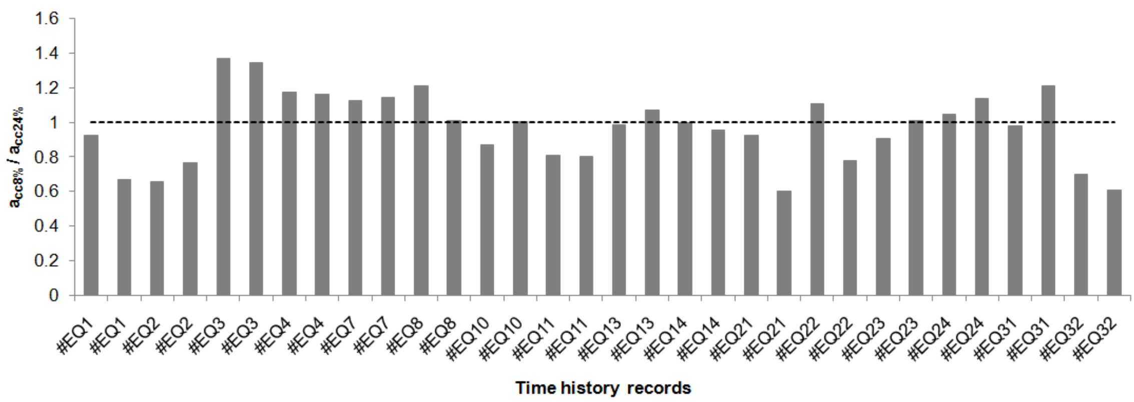

Fig. 29 Acceleration response ratio of HDRB-VL2 with β = 8 % and 24 % in Class 1 *a/v* ground motions

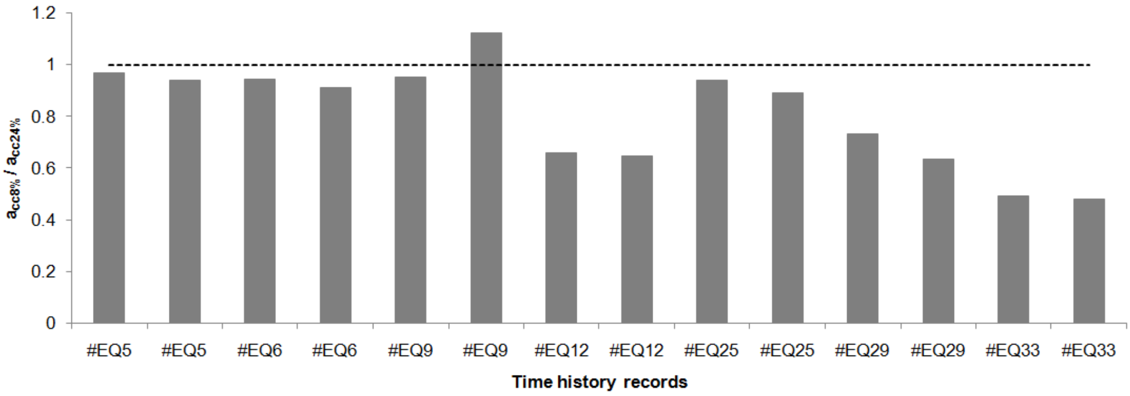

Fig. 30 Acceleration response ratio of HDRB-VL2 with β = 8 % and 24 % in Class 2 *a/v* ground motions

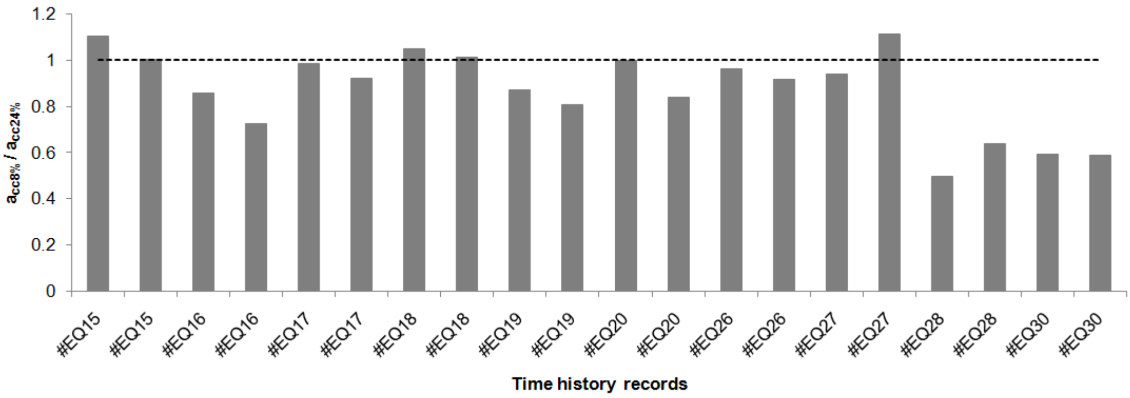

Fig. 31 Acceleration response ratio of HDRB-VL2 with β = 8 % and 24 % in Class 3 *a/v* ground motions

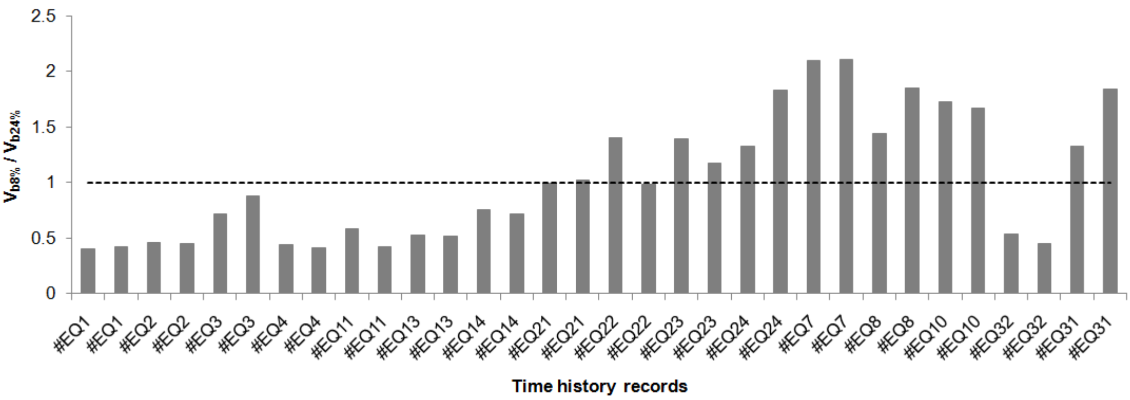

Fig. 32 Base shear ratio of HDRB-VL3 with β = 8 % and 24 % in Class 1 *a/v* ground motions

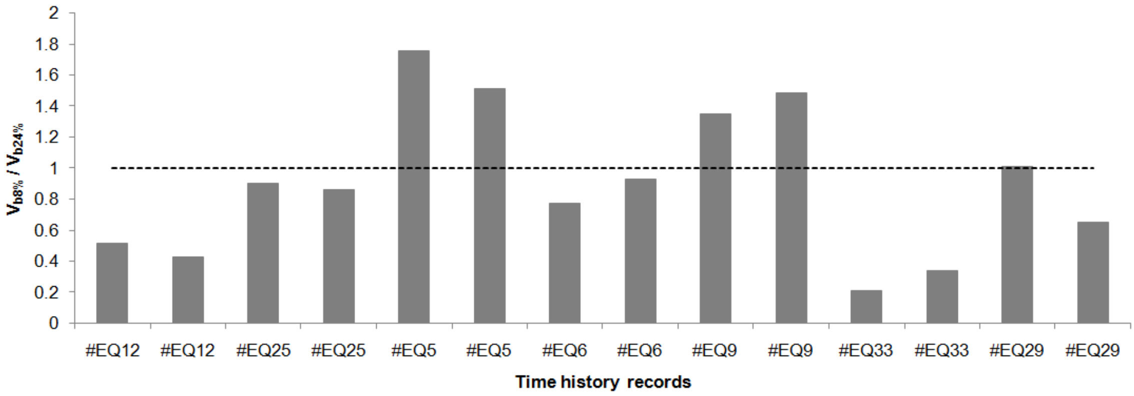

Fig. 33 Base shear ratio of HDRB-VL3 with β = 8 % and 24 % in Class 2 *a/v* ground motions

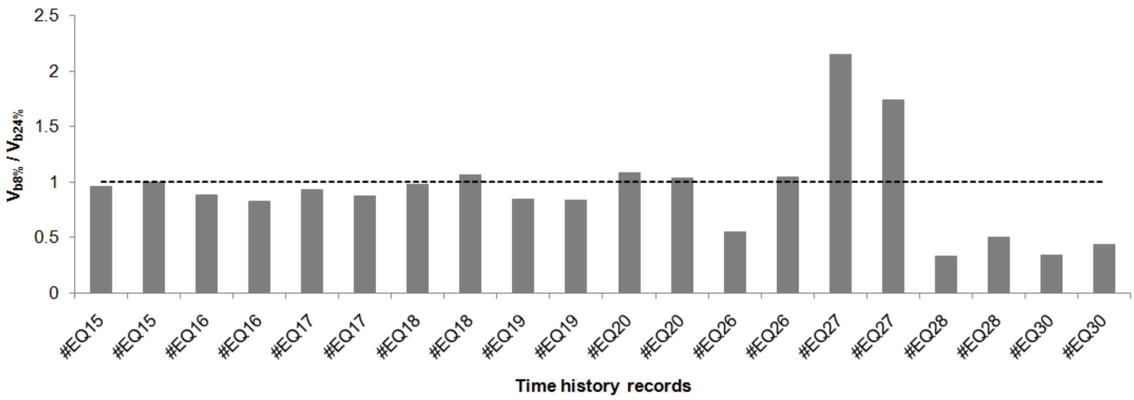

Fig. 34 Base shear ratio of HDRB-VL3 with β = 8 % and 24 % in Class 3 *a/v* ground motions

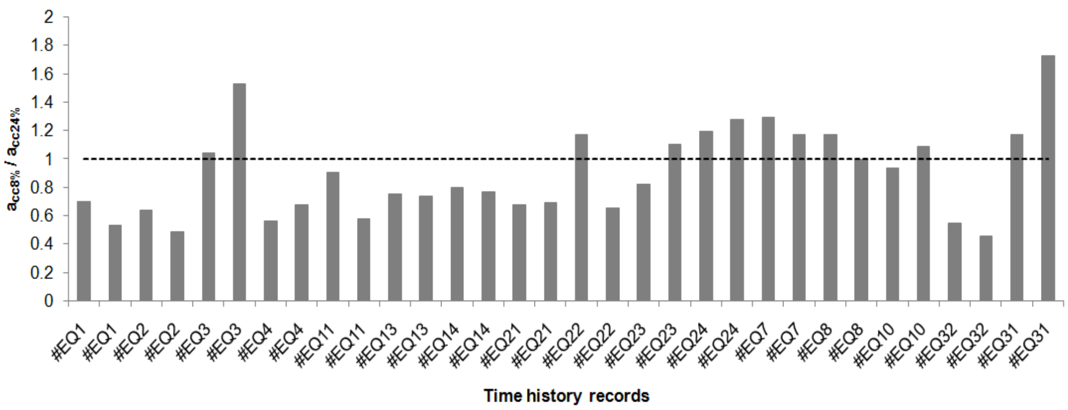

Fig. 35 Roof acceleration ratio of HDRB-VL3 with β = 8 % and 24 % in Class 1 *a/v* ground motions

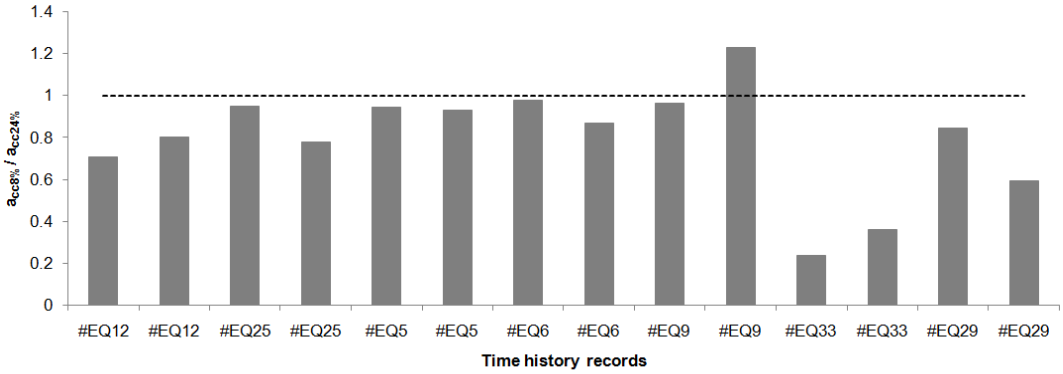

Fig. 36 Roof acceleration ratio of HDRB-VL3 with β = 8 % and 24 % in Class 2 *a/v* ground motions

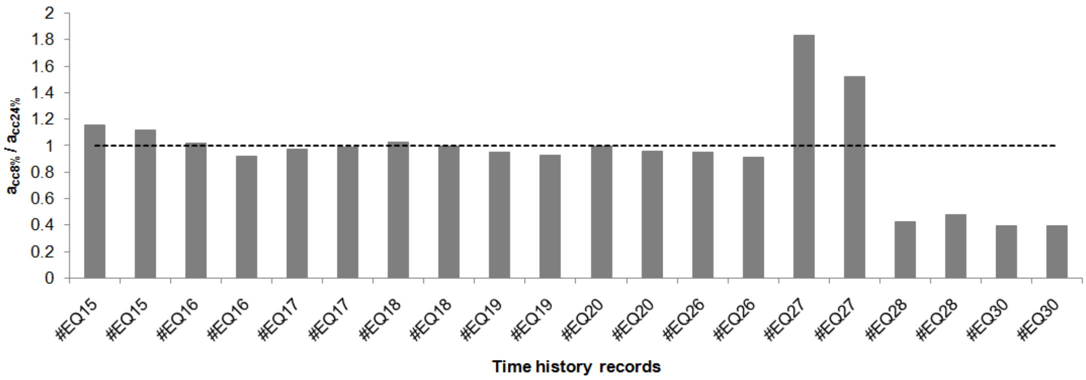

Fig. 37 Roof acceleration ratio of HDRB-VL3 with β = 8 % and 24 % in Class 3 *a/v* ground motions

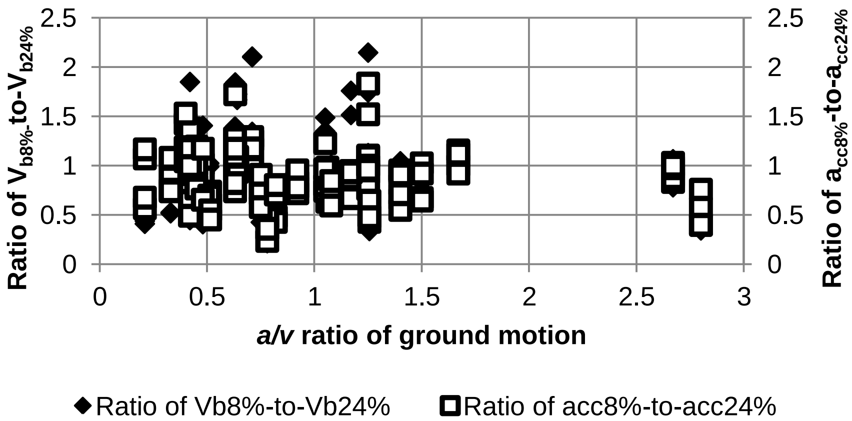

Fig. 38 Ratio of base shear and roof acceleration between β = 8 % and 24 % versus *a/v* ratio of ground motion

HDRB-VL3 except in few time histories such as Kobe earthquake. If such time history was used for seismic analysis of base isolation design, a higher damping ratio was preferred to reduce both base shear and acceleration response. However, as revealed in this study, this type of ground motion characteristic was very rare and among all the 33 time histories, only one possessed such obvious particular. Therefore, the equivalent-static design of base isolation structure using the constant-velocity spectra might underestimate the base shear demand because of the damping coefficient η.

5. Conclusions

Time history analyses of low-rise precast wall system, seismically-isolated using HDRB was performed in this study under 33 real earthquake records. Based on the study, the following conclusions are drawn:

- For very light superstructure such as HCPS-VL1 with large displacement demand, instability of HDRB might occur even though all design requirements of HDRB were met. The design limitation would cause the HDRB to become extremely sensitive and unstable to vertical loading as revealed in the compression test which observed twisting behaviour of the HDRB.Therefore, a guided or mobile mechanical pot bearing might be more suitable than HDRB in this kind of case.
- HDRB provided efficient seismic base isolation in terms of reducing base shear and floor acceleration demands when the *a/v* ratio of ground motion exceeds 0.5g/ms^{-1}, which was well below the currently classification criteria of 0.8g/ms^{-1}. Thus, the classification of Class 1 *a/v* ground motion according to NBCC (1985) using $0.8\ \text{g/ms}^{-1}$ could be lowered to $0.5\ \text{g/ms}^{-1}$ for effective base isolation design.
- Increasing damping ratio of base isolation system (i.e. through using lead rubber bearing, installation of additional damping mechanism at isolation interface or introducing modified rubber compound) did not reveal significant reduction in both base shear demand and roof acceleration in majority of the time history analyses particularly when the superstructure was having lower mass.

Acknowledgments

The research described in this paper was financially supported and sponsored by Doshin Rubber Products (M) Private Limited. Specially modified laboratory setup and assistance from the sponsor were also very much acknowledged. The authors would like to thank Universiti Teknologi Malaysia for the Research Student Grant (RSG) under the Tier 1 institutional funding.

References

Abrishambaf, A. and Ozay, G. (2010), “Effects of isolation damping and stiffness on the seismic behavior of structures”, *Proceedings of the Advances in Control, Chemical Engineering, Civil Engineering and Mechanical Engineering Conference, Tenerife, Spain, November-December*.

Ahmadi, H.R., Fuller, K.N.G. and Muhr, A.H. (1995), “Design and performance of high damping natural rubber base-isolators", *Proceedings of the 2nd International Conference on Seismology and Earthquake Engineering*, Tehran, Iran.

Bljuger, F. (1988). *Design of Precast Concrete Structures*, Ellis Horwood, West Sussex, England.

Braga, F. and Laterza, M. (2004), "Field testing of low-rise base isolated building", *Eng. Struct.*, **26**(11), 1599-1610.

British Standards Institution (1996), BS *6399: Loading for buildings. Part 1- Code of practice for dead and imposed loads*, British Standards Institution, London, UK.

CEN (2007), *EN 15129: Anti Seismic Devices*, British Standards Institution, London, UK.

CEN (2005), *BS EN 1337-3:2005 Structural Bearings – Part 3: Elastomeric Bearings,* British Standards Institution, London, UK.

Chung, W.J., Yun, C.B., Kim, N.S. and Seo, J.W. (1999), "Shaking table and pseudo-dynamic tests for the evaluation of the seismic performance of base-isolated structures", *Eng. Struct.*, **21**(4), 365-379.

Danila, G. (2013), "Seismic isolation systems for buildings subjected to Vrancea earthquakes", *Buletinul Institutului Politehnic Din Iaşi*, **9**(13), 91-102.

Danila, G., Chesca, A.B. and Petrescu, V. (2014), "Innovative method for buildings protection to seismic actions', *Bulletin of the Transilvania University of Braşov Series I: Engineering Sciences*, **7**(56), 63-70.

Elnashai, A.S. and Mcclure, D.C. (1996), "Effect of modeling assumptions and input motion characteristics on seismic design parameters of RC bridge piers", *Earthquake Engineering and Structural Dynamics*, **25**, 435-463.

Falborski, T. and Jankowski, R. (2012), "Shaking table experimental study on the base isolation sytem made of polymer bearings", *Proceedings of the 15th World Conference on Earthquake Engineering*, Lisbon, Portugal, September.

Forni, M. (2010), *Guidelines proposal for seismic isolation of nuclear power plant*. Unpublished note, Economic Development Ministry.

Hashemi, S.S., Tasnimi, A.A. and Soltani, M. (2009), "Nonlinear cyclic analysis of reinforced concrete frames, utilizing new joint element", *Scientia Iranica Transaction A: Civil Engineering*, **16**(6), 490-501.

Kelly, J.M. (1999), "The role of damping in seismic isolation", *Earthq. Eng. Struct. Dyn.*, **28**(1), 3-20.

Kelly, T.E. (2001), *Base Isolation of Structures: Design Guidelines*, Holmes Consulting Group Ltd, Wellington, NZ.

Kikuchi, M. and Aiken, I.D. (1997), "An analytical hysteresis model for elastomeric seismic isolation bearings", *Earthq. Eng. Struct. Dyn.*, **26**(2), 215-231.

Kubin, J., Kubin, D., Ozmen, A., Sadan, O.B., Eroglu, E., Sucuoglu, H. and Akkar, S. (2012). "Seismic Isolated Hospital Design Practice in Turkey: Erzurum Medical Campus", *Proceedings of the 15th World Conference on Earthquake Engineering*, Lisbon, Portugal, September.

Malek, K.A., Ahmadi, H.R., Muhr, A.H., Stephens, I.J., Gough, J., Picken, J.K., Lee, J.J., Zulkefli, M.U. and Taib, I.M. (2012), "Seismic protection of 2nd Penang Crossing using high damping natural rubber isolators", *Proceedings of the 15th World Conference on Earthquake Engineering*, Lisbon, Portugal, September.

Mayes, R.L. and Naeim, F. (2001), Chapter 14: Design of Structure with Seismic Isolation. In: Naeim, F. (Ed.) *The Seismic Design Handbook*, (2nd Edition), Kluwer Academic Pub, Boston.

Moroni, M.O., Sarrazin, M., Brull, J. and Munoz, R. (2006), "Shaking table tests of a scaled base isolated shear wall building", *Proceedings of the 8th US National Conference on Earthquake Engineering*, San Francisco, USA, April.

Naeim, K. and Kelly, J.M. (1999), *Design of Seismic Isolated Structures – From Theory to Practice,* John Wiley & Sons, New York, NY, USA.

NBCC (1985), *National Building Code of Canada 1985*, National Research Council of Canada, Ontario, Canada.

Politopoulos, I. (2008), "A review of adverse effects of damping in seismic isolation", *Earthq.Eng. Struct. Dyn.*, **37**(3), 447-465.

Sarrazin, M.J. (1992), "Design and construction of a building on seismic isolators", *Bull. IISEE*. **26**, 481-

497.
Sayani, P.J. (2009), "Relative performance comparison and loss estimation of seismically isolated and fixed-based buildings using PBEE approach", Ph.D. Dissertation, Utah State University, Utah.
Soudki, K.A., West, J.S., Rizkalla, S.H. and Blackett, B. (1996), "Horizontal connections for precast concrete shear wall panels under cyclic shear loading", *PCI J*., **41**(3), 64-80.
Taniwangsa, W. (2002), "Design considerations for a base isolated demonstration building", *Earthq*. *Spect*., **18**(4), 761-776.
Thurston, S.J. (2006), *Base Isolation of Low Rise Light and Medium-Weight Buildings*. Unpublished note, BRANZ.
Tiong, P.L.Y. (2014), "Performance of load-bearing precast concrete wall with base isolation subjected to seismic loadings", Ph.D. Dissertaion, Universiti Teknologi Malaysia, Skudai.
Tiong, P.L.Y., Adnan, A. and Hamid, N.H.A. (2013), "Behaviour factor and displacement estimation of low-ductility precast wall system under seismic actions", *Earthq*. *Struct*., **5**(6), 625-655.
Warn, G.P. and Ryan, K.L. (2012), "A review of seismic isolation for buildings: Historical development and research needs", *Build*., **2**, 300-325.
Wu, Y.M. and Samali, B. (2002), "Shake table testing of a base isolated model", *Eng*. *Struct*., **24**(9), 1203-1215.
Yoo, B. and Kim, Y.H. (2002), "Study on effects of damping in laminated rubber bearings on seismic responses for a 1/8 scale isolated test structure", *Earthq*. *Eng*. *Struct*. *Dyn*., **31**(10), 1777-1792.
Zhu, T.J., Heidebrecht, A.C. and Tso, W.K. (1988), "Effect of peak ground acceleration to velocity ratio on ductility demand of inelastic systems", *Earthq*. *Eng*. *Struct .Dyn*., **16**, 63-79.

IT